6-2014

A Seasonally Modulated Earthquake Swarm near Maupin, Oregon

Jochen Braunmiller
Oregon State University, jbraunmiller@usf.edu

John L. Nabelek
Oregon State University

Anne M. Trehu
Oregon State University

Geophysical Journal International

Geophys. J. Int. (2014) **197,** 1736–1743
Advance Access publication 2014 April 1

doi: 10.1093/gji/ggu081

A seasonally modulated earthquake swarm near Maupin, Oregon

Jochen Braunmiller,* John L. Nábělek and Anne M. Tréhu

College of Earth, Ocean and Atmospheric Sciences, Oregon State University, Corvallis, OR 97331*, USA. E-mail: jbraunmiller@usf.edu*

Accepted 2014 March 4. Received 2014 February 5; in original form 2013 October 9

SUMMARY

From December 2006 to November 2011, the Pacific Northwest Seismic Network (PNSN) reported 467 earthquakes in a swarm 60 km east of Mt Hood near the town of Maupin, Oregon. The swarm included 20 $M_D \geq 3.0$ events, which account for over 80 per cent of the cumulative seismic moment release of the sequence. Relocation of 45 $M_D \geq 2.5$ earthquakes and moment tensor analysis of nine $3.3 \leq M_w \leq 3.9$ earthquakes reveals right-lateral strike-slip motion on a north-northwest trending, 70° west dipping, 1 km^2 active fault patch at about 17 km depth. The swarm started at the southern end of the patch and migrated to the northwest at an average rate of 1–2 m d^{-1} during the first 18 months. Event migration was interrupted briefly in late 2007 when the swarm encountered a 10° fault bend acting as geometrical barrier. The slow migration rate suggests a pore pressure diffusion process. We speculate that the swarm was triggered by flow into the fault zone from upwards-migrating, subduction-derived fluids. Superimposed on the swarm is seasonal modulation of seismicity, with the highest rates in spring, which coincides with the maximum snow load in the nearby Cascade Mountains. The resulting surface load variation of about 4×10^{11} N km^{-1} arc length causes 1 cm annual vertical displacements at GPS sites in the Cascades and appears sufficient to modulate seismicity by varying normal stresses at the fault and fluid flow rates into the fault zone.

Key words: Earthquake dynamics; Earthquake source observations; Continental tectonics: strike-slip and transform; Dynamics and mechanics of faulting; Fractures and faults.

GJI Seismology

1 INTRODUCTION

Earthquake swarms lack a pronounced main shock, and their temporal evolution does not show a simple exponential aftershock decay rate (Mogi 1963). Recently, both natural (e.g. Vidale & Shearer 2006; Ibs-von Seht *et al.* 2008; Kato *et al.* 2010; Ruhl *et al.* 2010; Shelly & Hill 2011) and anthropogenic (e.g. Keranen *et al.* 2013) induced swarm activity has received renewed interest in part because of the possible connection between earthquake swarms and wastewater injection.

Seismicity east of the Cascade Mountains in SE Washington and NE Oregon is characterized by swarms with occasional large, damaging events like the magnitude $M = 6.1$ 1936 Milton-Freewater earthquake near the Oregon–Washington border (Wong & Bott 1995). Repeating swarm activity has been observed near the town of Maupin in northern central Oregon about 60 km E–SE of Mount Hood (Fig. 1). A series of earthquakes reaching moment magnitude $M_w = 4.6$ occurred in 1976 (Couch *et al.* 1976; Patton & Zandt 1991) and a minor swarm was observed in 1987. From 1987 until onset of the current swarm in December 2006, only about 2 events per year occurred in the area shown in Fig. 1. The current swarm was most active during 2007 and 2008, but continued, at diminished rate, until as recently as 2012 October 29. Understanding the origin of this unusually long-lived swarm can provide insights into the subsurface stress regime and factors that affect both natural and man-made earthquake swarms.

The current swarm has exceptionally been well recorded compared to earlier swarms in central and eastern Oregon due to the presence of the EarthScope Transportable Array (TA). During 2007, TA sites surrounded the otherwise sparsely instrumented region, and several sites, including TA site G06A (Fig. 1), are now permanent stations. We first present double-difference locations and regional moment tensor analysis to resolve the swarm's initial space–time evolution. Noting persistent seasonal modulation of seismicity throughout the duration of the Maupin swarm activity, we then analyse regional GPS and snow height measurements to investigate the effect of variable loading on the causative fault by seasonal snow accumulation in the nearby Cascade Mountains. Our analysis suggests that fluids play a crucial role in both generation and seasonal modulation of the Maupin earthquake swarm.

2 METHODS AND RESULTS

Earthquake hypocentres determined by the Pacific Northwest Seismic Network (PNSN) trend NNW within a 5 × 4 km^2 area and

*Now at: School of Geosciences, University of South Florida, Tampa, FL 33620, USA.

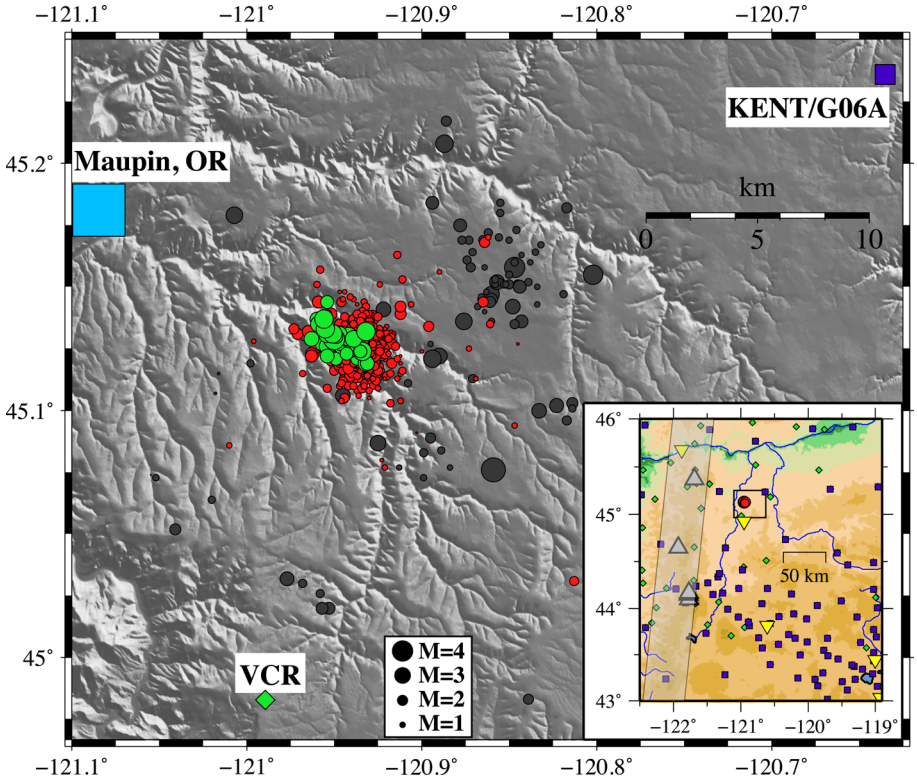

Figure 1. The Maupin swarm region with circles for earthquake epicentres from the 2006–2011 swarm in red and green (for 45 $M_D \geq 2.5$ events relocated in this study) and in black for 1970–2005 events; locations from PNSN. Light blue square: town of Maupin. Purple square: closest broad-band EarthScope TA station G06A (now permanent PNSN station KENT). Green diamond: closest short-period station VCR (installed 1983). The 1987 swarm location about 5 km ENE of the current swarm is likely real considering close recordings; the location of the 1976 swarm, possibly NE of the current one, is not well constrained (Couch *et al.* 1976). No Quaternary faults have been mapped for the map area (Weldon *et al.* 2003). Inset shows area of main map (rectangle); grey triangles are Cascade volcanoes with Mt Hood about 60 km WNW of the swarm (red circle); green diamonds and purple squares are short-period and broad-band seismic stations; yellow inverted triangles show location of PBO GPS sites shown in Fig. 5. Shaded area shows axis of maximum snow load in the Cascades (Fig. S6).

have depths of 12–24 km (Fig. 1). Waveforms at G06A (auxiliary Fig. S1), however, are very similar, suggesting a much smaller source area. We therefore manually picked *P* and *S* arrivals for all 45 earthquakes with duration magnitude $M_D \geq 2.5$ from seismic stations within 150 km epicentral distance. We visually checked picks at each station for consistency (i.e. picking the same phase onset) before locating individual events using hypoinverse (Klein 2011). The hypocentres tighten considerably and fall within a NNW-trending 2 × 1-km-long ellipse at 14–19 km depth. The formal 1σ absolute location uncertainties are about 1 km horizontally and 3 km vertically for the best locations but overlap completely. Varying the crustal model did not affect epicentres because of the good azimuthal station coverage. Depths changed by up to a few kilometre but consistently remained in the lower part of the seismogenic upper crust.

Next, we relocated the events relative to each other using hypoDD (Waldhauser & Ellsworth 2000) to determine their spatial relation. The results in map view and cross-section (Fig. 2, Table S1) show a small-source region at about 17 km depth with horizontal dimensions of about 0.8 × 0.4 km and less than 1 km range in depth. The relative locations are consistent with the absolute locations, but with uncertainties of less than 100 m horizontally and 200 m vertically (Table S1) relative positions are more reliable allowing for detailed analysis of the temporal and spatial evolution of activity.

We attempted full waveform regional moment tensor inversion for $M_D > 3.0$ events using the method of Nábělek & Xia (1995). Three-component seismogram inversion is performed at long periods ($T \geq 10$ s) where a simple 1-D crustal velocity model adequately describes propagation effects. The broad-band seismic stations provide excellent azimuthal coverage, and we obtained solutions for nine events (Fig. 2, Table S2). All have a strike-slip source mechanism with an N-NW trending, steeply (70°) west dipping nodal plane, which, based on the trend of hypocentres, is the likely fault plane. Waveform fits are excellent (Fig. S2) and source parameters (strike, dip, rake, depth and seismic moment) are well resolved (Fig. S3). All events have double-couple mechanisms and require no non-shear source components. Event centroid depths, obtained in 3 km steps, are consistent with hypoDD depths. Most events have a strike of about 165°. A 10° clockwise rotation for the 2008 April 5 and 2009 April 20 events is constrained by small, but significant, amplitude ratio changes (Fig. S4).

Within the small-source region (Fig. 2), the space–time evolution is resolved. The swarm started at the south end of the cluster and migrated NNW at 1–2 m d^{-1} until about mid-August 2007. The hypocentres (purple and blue in Fig. 2) and fault plane solutions of three larger events (2007 March 1, 2007 May 2 and 2007 June 14) are consistent with rupture on a ∼500-m-long, steeply WSW dipping, NNW trending (azimuth of 345°) fault segment at 17.0–17.4 km depth. Earthquake migration stalled temporarily near 45.127°N before continuing north in early 2008 and reaching a northern terminus by mid-2008. The average horizontal migration rate until then continued to be about 1 m d^{-1} and the vertical shoaling rate is about 0.5 m d^{-1}. The southern segment was reactivated by the strongest

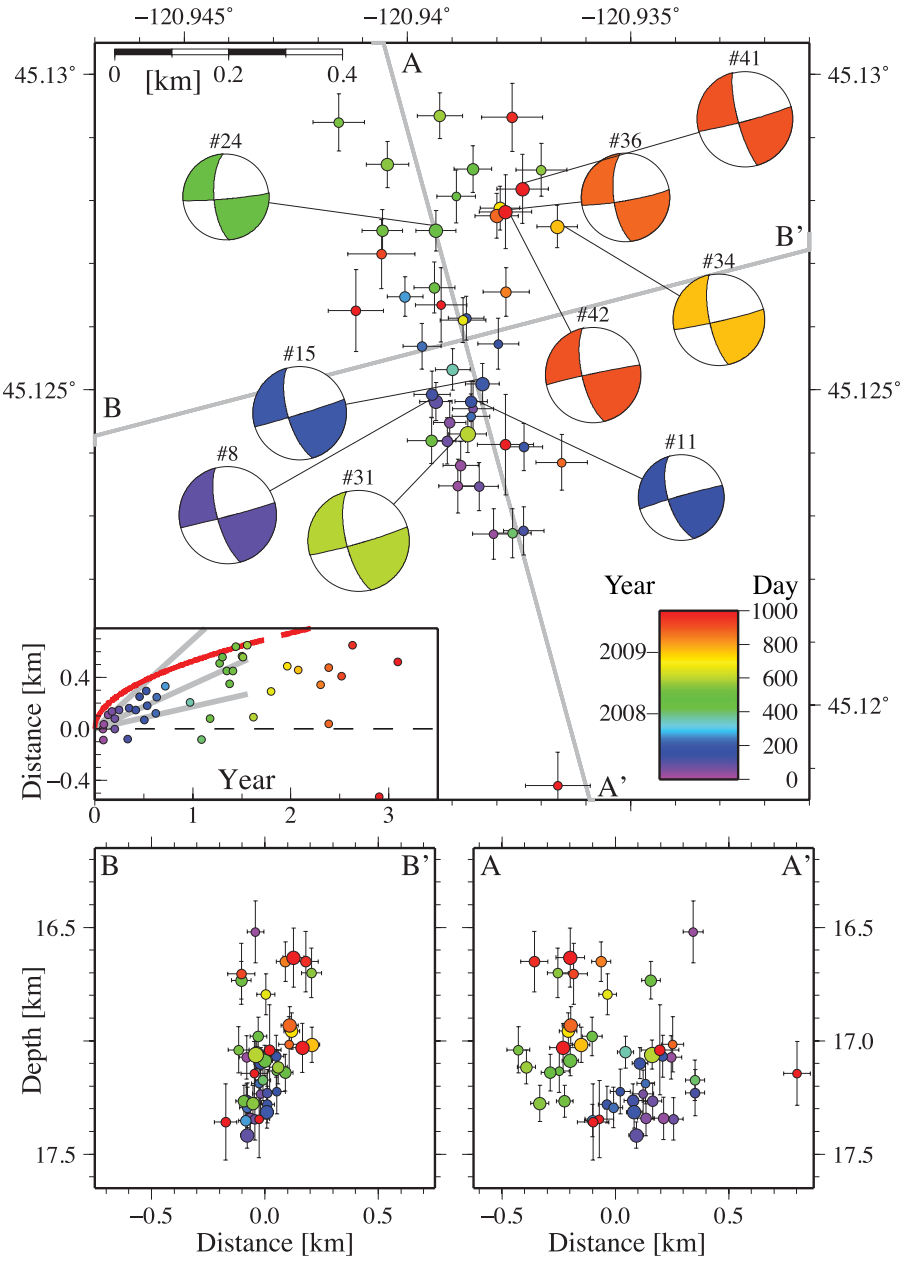

Figure 2. Map (top) and cross-sections (bottom; left B–B′, right A–A′) showing hypoDD relocations of 45 $M_D \geq 2.5$ events (coloured circles with formal 2σ uncertainties) and moment tensor solutions of nine events. Locations and source parameters are listed in Tables S1 and S2, respectively. Colour is chronological from day 0 (2006 December 1) to day 1000 (2009 August 27); later events are red. Map inset shows primarily northward event migration (positive values; distance is along A′–A with 0 at event #1); time in years since December 2006, grey lines are for 0.5, 1 and 2 m d^{-1} rates, respectively. Red line shows pore pressure perturbation triggering front from a fluid injection at distance = 0 and time = 0 for a diffusivity of 0.75×10^{-3} m^2 s^{-1}, solid for period of observed northward migration (about 1.5 yr); triggering can happen after the pore pressure perturbation reaches a space–time point, that is, at or behind the red line (see Shapiro *et al.* 1997 for details). Distance in cross-sections is relative to average event location (45.1258°N, 120.9387°W).

event on 2008 July 14 ($M_w = 3.9$) and has been intermittently active afterwards.

The northern segment has a length of about 300 m, dips steeply to the W and trends northerly (355°) based on fault plane solutions for the 2008 April 5 and 2009 April 20 events. A 10° clockwise rotation between segments indicates a fault bend that could have caused stalling. The northern segment remained active and is wider (E–W) than the southern segment, consistent with the events' larger depth range (16.5–17.3 km) on a 70°-dipping fault. The nodal planes of events on the eastern part of the northern segment (2008 December 27, and 2010 January 2 and 2010 December 30) trend approximately 347°, similar to events on the southern segment, and are slightly shallower than events to the west suggesting activity on a slightly non-planar fault.

The temporal evolution shows the swarm character (Figs 3 and 4). The cumulative number of earthquakes versus time (blue line, Fig. 3) does not follow typical main shock–aftershock decay where the number of aftershocks per time decreases exponentially after a

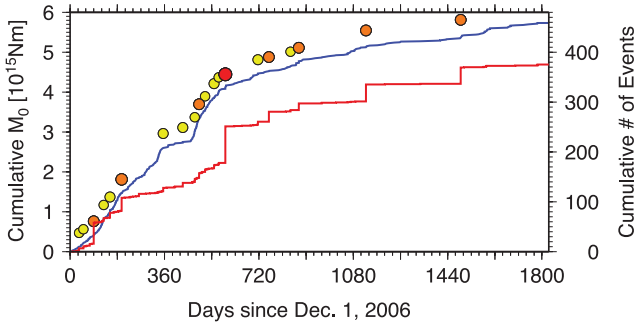

Figure 3. Temporal swarm evolution (December 2006 to November 2011) shows cumulative number of events (blue) and seismic moment release (red); circles mark times of $M_D \geq 3$ earthquakes ($\geq$3.0, $\geq$3.5 and $\geq$4.0 are yellow, orange and red, respectively; M_D is PNSN duration magnitude) and are offset from the blue line to show times of elevated seismicity are not simply aftershock sequences of larger events. Event seismic moments are from moment tensor analysis for nine events (Table S2) and from cross-correlation analysis of G06A waveforms (see auxiliary material) for all others.

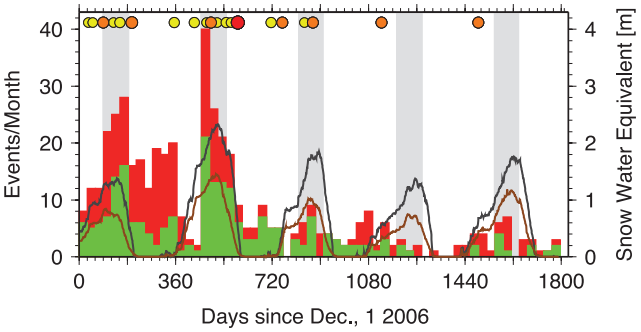

Figure 4. The distribution of events per month (red: all events; green: $M_D \geq 1.6$ for which the PNSN catalogue is roughly complete) shows a seasonal pattern with elevated seismicity during March–May (highlighted by grey boxes), which coincides with the largest snow pack in the Cascade Mountains. Black shows snow water equivalent (SWE) for a USDA SNOwpack TELemetry (SNOTEL) site near Mt Hood, Oregon, at ~1600 m elevation (Fig. S6), and brown is SWE averaged over 32 SNOTEL sites in the western Cascades above 1100 m elevation (Fig. S6). Circles mark $M_D \geq 3$ events as in Fig. 3.

main shock. Instead, larger events (coloured circles are 20 $M_D \geq 3$ events) occurred throughout the swarm and periods of elevated seismicity, for example, starting in early March 2008 (day 458), are generally not 'typical' aftershocks. In this example, the largest event on 2008 July 14 (day 591) actually marks the end of a high seismicity period. Overall, swarm activity has markedly declined since mid-2008 when 0.6 events per day were observed. Since early 2010 (day 1127), seismicity rate has been 0.06 events per day, still a factor of 10 above the 1987–2006 interswarm rate before reaching the background level again in November 2011.

The final cumulative seismic moment (red line in Fig. 3) of 4.7×10^{15} Nm is equivalent to $M_w = 4.4$. Though mainly due to 20 $M_D \geq 3$ events (>80 per cent of moment release), it is not dominated by a single main shock. The moment sum corresponds to about 0.1 m cumulative slip assuming a 1 km^2 fault area and rigidity $\mu = 4 \times 10^{10}$ N m^{-2}. Cumulative moment is based on moment magnitudes M_w, which were estimated for each event taking advantage of G06A waveform similarity (see auxiliary material). The frequency–magnitude relation (Fig. S5) has *a b* value of 0.95 $\pm$ 0.03 close to $b = 1.0$ often found in tectonic areas (Frohlich & Davis 1993) and lower than for volcanic or magmatic swarms, which can reach $b = 3.0$ (McNutt 2005).

3 DISCUSSION AND SUMMARY

The 17 km depth of the Maupin swarm is deep compared to most other crustal earthquake swarms worldwide and likely occurs at the base of the seismogenic part of the crust. Its depth though is consistent with depths reached by other earthquakes in the region because of the mafic composition of the crust, which allows relatively deep crustal brittle deformation. However, deep swarms within the nominally aseismic lower crust have been observed in volcanic regions and are thought to be associated with magma emplacement (Smith *et al.* 2004; White *et al.* 2011) or ascending CO_2 released by underlying magma (Shelly & Hill 2011). The observed slow event migration rate for Maupin points to a pore pressure diffusion process suggesting that swarm onset was triggered by fluid flow into and through the affected area (e.g. Shapiro *et al.* 1997). An increase in pore fluid pressure brings material closer to failure by moving the Mohr circle closer to the Mohr–Coulomb failure criteria. In a critically pre-stressed area, a small increase in pore pressure can cause failure.

At 17 km depth, triggering by inflow of meteoritic water from the Cascades or other sources seems unlikely assuming normal crustal permeability (Saar & Manga 2004) and the 10 s of years estimated residence time of shallow thermal waters in the Cascades (Ingebritsen *et al.* 1994). The double-couple source mechanisms are inconsistent with direct stressing due to a magmatic intrusion event at the depth of the earthquakes themselves, but do not entirely rule out the possibility for such an intrusion. The closest GPS site about 22 km south of the swarm region (site P063 shown in Fig. 5) shows no unusual displacement that could be associated with an intrusion suggesting an intrusion had to be either quite deep and farther away or small (though the site's location due south would be quite insensitive to an intrusion along an NNW-SSE trending strike-slip fault). We thus prefer a fluid pulse from a deeper magmatic source, which migrated upward through the ductile lower crust and triggered seismicity in a critically pre-stressed region when it reached the bottom of the seismogenic crust.

Triggering by aqueous fluids exsolved from a deeper magma intrusion has been described for crustal swarms near Lake Tahoe (von Seggern *et al.* 2008) and Yellowstone (Shelly *et al.* 2013) and has been proposed as driving mechanism for NW Bohemia/Vogtland swarms (Geissler *et al.* 2005), where spring water shows isotopic evidence for mantle-derived fluids (Bräuer *et al.* 2003). In the central Oregon Cascades region, the magmatic effects of subduction extend roughly 50–75 km to the east of the crest of the Cascades. Geochemical evidence for degassing due to magma intrusion has been found in a spring about 70 km south of the Maupin swarm and also further south (James *et al.* 1999). Additional evidence for magmatic aqueous fluids in the lower crust and uppermost mantle in this region comes from observations of high electrical conductivities (Meqbel *et al.* 2014).

The Maupin seismicity shows seasonal variability superimposed on overall swarm evolution. The event-per-month distribution (Fig. 4) has pronounced maxima during spring (March–May) when, overall, more than twice as many events occur than for any other quarter (December–February, June–August, September–November). Following Christiansen *et al.* (2005), we applied a one-way ANOVA variance test to determine the significance of the

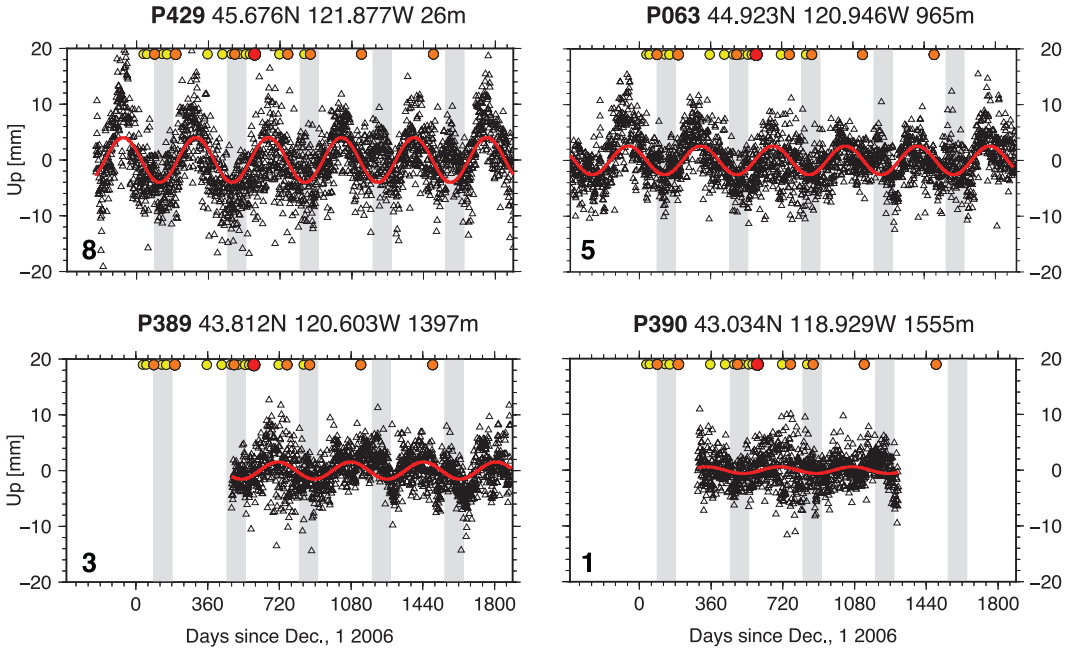

Figure 5. Snow load causes an annual vertical deformation signal that decays with distance from the Cascade Mountains. Shown are vertical component PBO GPS data for a west-to-east transect from the Cascades (P429) to P063 near Maupin and into southeastern Oregon (P389, P390). Site locations are shown in Fig. 1 inset; sites in southeastern Oregon were chosen to avoid mountainous regions due east of Maupin (the snow load in the Ochoco and Wallowa Mountains generates local vertical deformation). The red line is best fit sine function to data (triangles) after mean and trend removal. Maximum depression occurs during the March–May period (highlighted by grey boxes) when snow load is maximal and decays from west (8-mm peak-to-peak amplitude, number in lower left of each panel) to east (1 mm) similar to observations in Japan (Heki 2001). Circles mark $M_D \geq 3$ events as in Fig. 3.

excess activity. Considering overall decay in swarm activity since mid-2008, we normalized each 1-yr period (December to November) such that the quarter with most events for a given 1-yr period is set to 1; the normalized number of events per quarter thus varies from 0 to 1. For the 5-yr observation period, which admittedly is short for a statistical analysis that is trying to find an annual pattern, we found that excess activity during the March–May quarter is significant at the 95 per cent level. Seasonality was strongest in 2007 and 2008, when the swarm was most active, and weakened as the level of activity decreased. Seasonality was not observed during 2010, the year with the lowest snow load in the Cascade Mountains (Fig. S6), which may suggest that triggering and its efficiency are linked to snowpack. We note that the recording network capability stayed essentially the same throughout the swarm and observed seasonal seismicity modulation is not an artefact of seasonal station outages.

An annual seismicity signal is difficult to explain by a subterranean source, suggesting a surficial driving force. Seasonally modulated seismicity has been observed in western North America near volcanic areas (Gao *et al.* 2000; Saar & Manga 2003; Christiansen *et al.* 2005), in the Coastal Mountains of Alaska–British Columbia (Wolf *et al.* 1997), and along the San Andreas strike-slip system (Christiansen *et al.* 2007) as well as in Japan (e.g. Heki 2001, 2003) and in the Nepal Himalaya (Bollinger *et al.* 2007; Bettinelli *et al.* 2008). These studies investigated groundwater recharge, snow loading/unloading and seasonal barometric changes as possible causes for annual signals because they can generate stress changes on the order of 0.01–0.1 MPa in the source area, which is considered a minimum value necessary to generate earthquake rupture (e.g. Harris 1998 and related papers in special section of J. Geophys. Res.). Rupture initiation by such small stress changes implies that the affected faults are near critically stressed.

The annual peak in seismicity of the Maupin swarm correlates with maximum snow load in the Cascade Mountains about 50–120 km west of the swarm (Figs 4 and S6) suggesting a causal relationship. The average snow water equivalent height in the 70-km-wide mountain strip of the Cascades during March–May is about 0.6 m (Figs 4 and S6), resulting in a load of about 4×10^{11} N km^{-1} along strike of the Cascades. The snow load corresponds to a surface pressure variation of about 6 kPa resulting in a peak-to-peak annual vertical displacement of about 1 cm at GPS sites in the Cascades (Fig. 5). The amplitude of the GPS signal and its decay with increasing distance from the Cascades is similar to observations from Japan with comparable snow load (Heki 2001).

Stress changes in the crust due to a surface load can act in two ways to instantaneously enhance seismicity. Increased normal stress directly beneath a linear load moves strike-slip faults parallel to the load axis away from failure; this mechanism has been invoked to explain an increase in large intraplate earthquake activity in Japan during summer (Heki 2003) when snow load is absent. For faults at crustal depths located 10 s of km away from a load, however, normal stress decreases slightly (on the order of 1 kPa or less, Fig. 6; Heki 2003), which leads to slight fault unclamping when the load is maximum. A similar hydrological loading/unloading mechanism has been invoked to attribute seasonal seismicity variations in the Himalaya to the monsoon in the Ganges basin (Bettinelli *et al.* 2008). In addition to bringing the fault closer to failure, we postulate that the load also leads to simultaneous compression (on the order of 1 kPa, Fig. 6) of fluid conduits at greater depth, which drives fluids rapidly upward into the Maupin source region. A combination of conduit squeezing and fault unclamping could explain the annual seismicity variations. In our case, swarm triggering is due to fluid injection and is not subject to the stress considerations discussed

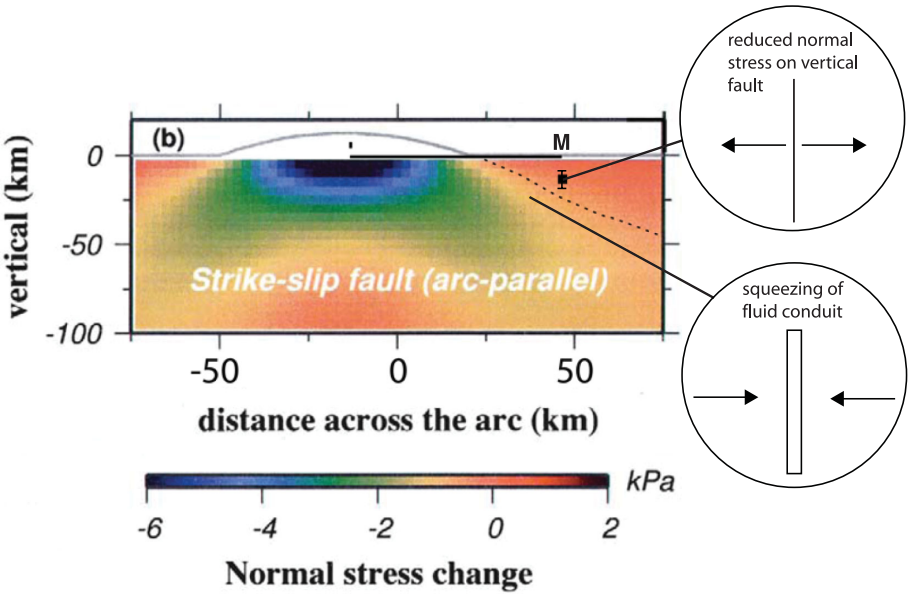

Figure 6. Normal stress and pressure changes (compressions are negative) on a vertical strike-slip fault [striking load (arc) parallel] and a vertical conduit, respectively. Modified from Heki (2003). Snow load (solid line) is 70 km wide and Maupin (labelled M) is 25 km east of snow load edge (and about 60 km east of the snow load maximum); the maximum snow water equivalent is 1 m. Square is source region. Dashes approximate transition from compression to tension. Circles show schematic illustrations of fault unclamping and fluid expulsion from the zone of compression.

above, while the small stress changes due to the snow load only act to modulate seismicity.

Although elevated early fall seismicity at about 5 km depth south of Mt Hood has been attributed to peak run-off from melting snow in spring, with a 5-month lag because of pore pressure diffusion (Saar & Manga 2003), we consider this an unlikely mechanism for modulating seismicity near Maupin because of arguments cited above against a periodic meteoritic fluid source at the hypocentre depth. Moreover, the effect of pore pressure diffusion, which decays exponentially with depth (Saar & Manga 2004), is negligible at 17 km depth for the low diffusivity suggested by the very slow event migration (Fig. 2). Other factors that could affect surface load annually in the epicentre area, such as variations in groundwater level, soil moisture and vegetation, are probably insignificant in the semi-arid region east of the Cascades, and snow cover in the Maupin area itself is negligible (Fig. S6).

Since November 2011, seismicity in the Maupin area has returned to pre-swarm levels of about 2 events per year. We assume that the swarm was fluid triggered. The active fault patch was critically stressed and began to fail seismically when fluid influx reduced fault strength. Continued fluid influx and high pore fluid pressure kept the fault rupturing in small earthquakes until the stress on the fault had been nearly completely released. Activity during the swarm appears to have been modulated by snowpack, suggesting that small, periodic regional stress changes due to changes in snowpack height suffice to modify seismicity.

ACKNOWLEDGEMENTS

We thank the PNSN, USArray and IRIS DMC staff for USArray and PNSN data; M. Fouch and D. James for access to High Lava Plains data; UNAVCO staff for GPS data and K. Heki, L. Bollinger, J. Vidale and associate editor D. Agnew for reviews. Snow water equivalents are from USDA Natural Resource Conservation Service automated SNOwpack TELemetry (SNOTEL) sites. DEM data are from the USGS' National Elevation Database. Figures were generated with GMT (Wessel & Smith 1998). This research has been supported by NSF grants OCE0752598, EAR0550402, EAR0719204 and EAR0952396.

REFERENCES

Bettinelli, P., Avouac, J.P., Flouzat, M., Bollinger, L., Ramillien, G., Rajaure, S. & Sapkota, S., 2008. Seasonal variations of seismicity and geodetic strain in the Himalaya induced by surface hydrology, *Earth planet. Sci. Lett.,* **266,** 332–344.

Bollinger, L., Perrier, F., Avouac, J.-P., Sapkota, S., Gautam, U. & Tiwari, D.R., 2007. Seasonal modulation of seismicity in the Himalaya of Nepal, *Geophys. Res. Lett.,* **34,** L08304, doi:10.1029/2006GL029192.

Bräuer, K., Kämpf, H., Strauch, G. & Weise, S.M., 2003. Isotopic evidence (^{3}He/^{4}He, $^{13}C_{CO2}$) of fluid-triggered intraplate seismicity, *J. geophys. Res.,* **108**(B2), ESE3.1–ESE3.11.

Christiansen, L.B., Hurwitz, S. & Ingebritsen, S.E., 2007. Annual modulation of seismicity along the San Andreas Fault near Parkfield, CA, *Geophys. Res. Lett.,* **34,** L04306, doi:10.1029/2006GL028634.

Christiansen, L.B., Hurwitz, S., Saar, M.O., Ingebritsen, S.E. & Hsieh, P.A., 2005. Seasonal seismicity at western United States volcanic centers, *Earth planet. Sci. Lett.,* **240,** 307–321.

Couch, R., Trasher, G. & Keeling, K., 1976. The Deschutes Valley earthquake of April 12, 1976, *Ore Bin,* **38,** 151–161.

Frohlich, C. & Davis, S., 1993. Teleseismic b-values: or much ado about 1.0, *J. geophys. Res.,* **98,** 631–644.

Gao, S.S., Silver, P.G., Linde, A.T. & Sacks, I.S., 2000. Annual modulation of triggered seismicity following the 1992 Landers earthquake in California, *Nature,* **406,** 500–505.

Geissler, W.H. *et al.*, 2005. Seismic structure and location of a CO_2 source in the upper mantle of the western Eger (Ohre) rift, central Europe, *Tectonics,* **24,** TC5001, doi:10.1029/2004TC001672.

Harris, R.A., 1998. Introduction to special section: stress triggering, stress shadows, and implications for seismic hazard, *J. geophys. Res.,* **103,** 24 347–24 358.

Heki, K., 2001. Seasonal modulation of interseismic strain buildup in northeastern Japan driven by snow loads, *Science,* **293,** 89–92.

Heki, K., 2003. Snow load and seasonal variation of earthquake occurrence in Japan, *Earth planet. Sci. Lett.,* **207,** 159–164.

Ibs-von Seht, M., Plenefisch, T. & Klinge, K., 2008. Earthquake swarms in continental rifts – a comparison of selected cases in America, Africa, and Europe, *Tectonophysics,* **452,** 66–77.

Ingebritsen, S.E., Mariner, R.H. & Sherrod, D.R., 1994. Hydrothermal systems of the Cascades range, north-central Oregon, Open-File Rep, *U.S. Geol. Surv. Prof. Pap.,* **1044-L,** 86 pp.

James, E.R., Manga, M. & Rose, T.P., 1999. CO_2 degassing in the Oregon Cascades, *Geology,* **27,** 823–826.

Kato, A., Sakai, S., Iidaka, T., Iwasaki, T & Hirata, N., 2010. Non-volcanic seismic swarms triggered by circulating fluids and pressure fluctuations above a solidified diorite intrusion, *Geophys. Res. Lett.,* **37,** doi:10.1029/2010GL043887.

Keranen, K.M., Savage, H.M., Abers, G.A. & Cochran, E.S., 2013. Potentially induced earthquakes in Oklahoma, USA: links between wastewater injection and the 2011 M_w 5.7 earthquake sequence, *Geology,* **41,** 699–702.

Klein, F.W., 2011. User's guide to HYPOINVERSE-2000, a Fortran program to solve for earthquake locations and magnitudes, USGS Open File Report 02-171 revised.

McNutt, S.R., 2005. Volcanic seismology, *Annu. Rev. Earth planet. Sci.,* **33,** 461–491.

Meqbel, N.M., Egbert, G.D., Wannamaker, P.E., Kelbert, A. & Schultz, A., 2014. Deep electrical resistivity structure of the Northwestern U.S. derived from 3-D inversion of USArray magnetotelluric data, *Earth planet. Sci. Lett.,* doi:10.1016/j.epsl.2013.12.026.

Mogi, K., 1963. Some discussions on aftershocks, foreshocks, and earthquake swarms – the fracture of a semi-infinite body caused by an inner stress origin and its relation to the earthquake phenomena, *Bull. Earthq. Res. Inst.,* **41,** 615–658.

Nábělek, J. & Xia, G., 1995. Moment-tensor analysis using regional data: application to the 25 March, 1993, Scotts Mills, Oregon, earthquake, *Geophys. Res. Lett.,* **22,** 13–16.

Patton, H.J. & Zandt, G., 1991. Seismic moment tensors of western U.S. earthquakes and implications for the tectonic stress field, *J. Geophys. Res.,* **96,** 18 245–18 259.

Ruhl, C., Bilek, S.L. & Stankova-Pursley, J., 2010. Relocation and characterization of the August 2009 microearthquake swarm above the Socorro magma body in the central Rio Grande Rift, *Geophys. Res. Lett.,* **37,** L23304, doi:10.1029/2010GL045162.

Saar, M.O. & Manga, M., 2003. Seismicity induced by seasonal groundwater recharge at Mt. Hood, Oregon, *Earth planet. Sci. Lett.,* **214,** 605–618.

Saar, M.O. & Manga, M., 2004. Depth dependence of permeability in the Oregon Cascades inferred from hydrogeology, thermal, seismic, and magmatic modeling constraints, *J. geophys. Res.,* **109,** B04204, doi:10.1029/2003JB002855.

Schurr, B. & Nábělek, J., 1999. New techniques for the analysis of earthquake sources from local array data with an application to the 1993 Scotts Mills, Oregon, aftershock sequence, *Geophys. J. Int.,* **137,** 585–600.

Shapiro, S.A., Huenges, E. & Born, G., 1997. Estimating the crust permeability from fluid-injection-induced seismic emission at the KTB site, *Geophys. J. Int.,* **131,** F15–F18.

Shelly, D.R. & Hill, D.P., 2011. Migrating swarms of brittle-failure earthquakes in the lower crust beneath Mammoth Mountain, California, *Geophys. Res. Lett.,* **38,** L20307, doi:10.1029/2011GL049336.

Shelly, D.R., Hill, D.P., Massin, F., Farrell, J. & Smith, R.B., 2013. A fluid-driven earthquake swarm on the margin of the Yellowstone caldera, *J. Geophys. Res.,* **118,** 1–15.

Smith, K.D., v. Seggern, D., Blewitt, G., Preston, L., Anderson, J.G., Wernicke, B.P. & Davis, J.L., 2004. Evidence of deep magma injection beneath Lake Tahoe, Nevada-California, *Science,* **305,** 1277–1280.

Vidale, J.E. & Shearer, P.M., 2006. A survey of 71 earthquake bursts across southern California: exploring the role of pore fluid pressure fluctuations and aseismic slip as drivers, *J. geophys. Res.,* **111,** B05312, doi:10.1029/2005JB004034.

von Seggern, D.H., Smith, K.D. & Preston, L.A., 2008. Seismic spatial-temporal character and effects of a deep (25–30 km) magma intrusion below North Lake Tahoe, California-Nevada, *Bull. seism. Soc. Am.,* **98,** 1508–1526.

Waldhauser, F. & Ellsworth, W.L., 2000. A double-difference earthquake location algorithm: method and application to the Northern Hayward fault, California, *Bull. seism. Soc. Am.,* **90,** 1353–1368.

Weldon, R.J. II, Fletcher, D.K., Weldon, E.M., Scharer, K.M. & McCrory, P.A., 2003. An update of Quaternary faults of central and eastern Oregon, U.S. Geol. Surv. Open-File Report 02-301.

Wessel, P. & Smith, W.H.F., 1998. New, improved version of generic mapping tools released, *EOS, Trans. Am. geophys. Un.*, **79,** 579.

White, R.S., Drew, J., Martens, H.R., Key, J., Soosalu, H. & Jakobsdóttir, S.S., 2011. Dynamics of dyke intrusion in the mid-crust of Iceland, *Earth planet. Sci. Lett.,* **304,** 300–312.

Wolf, L.W., Rowe, C.A. & Horner, R.B., 1997. Periodic seismicity near Mt. Ogden on the Alaska-British Columbia border: a case for hydrologically triggered earthquakes? *Bull. seism. Soc. Am.,* **87,** 1473–1483.

Wong, I.G. & Bott, J.D.J., 1995. A look back at Oregon's earthquake history, 1841–1994, *Oregon Geol.,* **57,** 125–139.

SUPPORTING INFORMATION

Additional Supporting Information may be found in the online version of this article:

Figure S1. Vertical component waveforms for station G06A for 43 relocated $M_D \geq 2.5$ events (data not available for event #38 and noisy for event #9, Table S1) in the 0.7–1.8 Hz passband. Traces are scaled and aligned relative to largest *P* amplitude (at 1.7 s) and include *S* waves. Note waveform similarity and the consistent *S–P* arrival time difference. Left: traces in chronological order. Right: traces sorted by event latitude.

Figure S2. Moment tensor waveform fit example, event #15 (14 June 2007). Shown are vertical, radial and transverse component observed (black) and synthetic (red) seismograms used for moment tensor inversion. Stations are in azimuthal order; numbers beneath station code are event-station azimuth and distance. Triangles on fault plane solution illustrate excellent azimuthal coverage. Inversion was performed in the 10–30 s band. Grey station codes are TA sites and black permanent sites; the PNSN has 'adopted' 20 TA sites significantly expanding broad-band station coverage in the Pacific Northwest, for this event, 10 such sites were used.

Figure S3. Source parameter resolution example, event #15 (14 June 2007). Left: Normalized variance versus centroid depth. Best depth is at 15 km; 5 per cent variance increase corresponds to [−3, 7] km bounds. Mechanism is stable over wide depth range. Right: Variance relative to best double couple solution (0° deviation) when one parameter is varied, 5 per cent variance increase corresponds to ±6°, ±10° and ±10° bounds for strike, dip and rake, respectively.

Figure S4. A ∼10° clockwise *T*-axis rotation for events #24 (2008 April 5) and #36 (2009 April 20), located in the northern swarm area relative to events in the southern area, is constrained by waveform differences, for example, different *Z*/*T* amplitude ratios at site G06A. Waveforms are $T \geq 10$ s, black observed, coloured synthetics (top: #15, 2007 June 14 in blue, bottom: #24 in green). Colours are as in Fig. 2.

Figure S5. Top: Histogram of events versus M_w. M_w is from cross correlation except for nine events with moment tensor solution, the preferred size estimate (Table S2). Inset: Comparison of coda duration magnitude M_D (PNSN) versus M_w from cross-correlation analysis for 459 events (red circles). Solid black line is one-to-one relation; green line is relation from Schurr & Nábělek (1999) derived for a western Oregon sequence, which fits the Maupin data well. Bottom: Frequency magnitude relation: $b = 0.95 \pm 0.03$ was derived in the $1.7 \leq M_w \leq 3.5$ range (solid line). Note lack of

$2.6 < M_w < 3.0$ events; dashed lines show regressions for $1.7 \leq M_w \leq 2.6$ and $3.0 \leq M_w \leq 3.5$, respectively, resulting both in $b = 1.2$.

Figure S6. Top: Map of SNOTEL sites (circles, larger circle: Mt Hood site shown in Fig. 4; colour code as in bottom part of this figure) relative to Maupin swarm (black square). Bottom: Snow water equivalent (SWE) heights in the western Cascades (blue colours: site averages for ≤900 m elevation and for five groups of sites binned in 200-m elevation increments above 900 m elevation), in the Cascades east of the divide (green) and in central Oregon (orange). SWE in the Maupin area is negligible since Maupin is at an elevation about 1000 m lower than the central Oregon sites shown in orange. The average SWE height in the Cascades in the highlighted strip on the map and above 800 m elevation, which is about 70 km wide, is about 0.6 m during the March–May period equivalent to a 6 kPa pressure increase or an integrated load of 4×10^{11} N km^{-1} along strike of the Cascade Mountains.

Table S1. HypoDD relocation of 45 earthquakes shown in Fig. 2.

Table S2. Regional moment tensor solutions for nine earthquakes shown in Fig. 2 (http://gji.oxfordjournals.org/lookup/suppl/doi:10.1093/gji/ggu081/-/DC1).